International Journal of Engineering Research (ISSN : 2319-6890)
Volume No.2, Issue No.3, pp : 214-219 01 July 2013

Optimization of Vibration Energy Harvesting on Wind-Spear

S. Nagakalyan[1], B. Raghu Kumar[2], K. V. Abhilash[3]

[1&3] Department of Mechanical Engineering, GITAM University, Hyderabad campus India

[2]Department Mechanical Engineering Department, K. L. University Vijayawada, India.

snagakalyan@gitam.edu

ABSTRACT: This analysis shows that, the coordinated Switch Harvesting on Inductor topology is higher in output power at small vibrations at 1 Hz. The recital of the topology at a frequency of 1 Hz and output power levels around 10 µW was found to positive and negative with the peak detection control circuit performance. The sample showed to increase the output power by a factor of two, compared to the standard full bridge rectifier, but when accounting for the control circuit power consumption of 13.2µW the gained output power was lost. The control circuit showed to be more of a limiting factor than expected and a set of requirements for a new control circuit was made. At higher energy levels the sample is expected to increase the output energy by up to 10 times and to extend the range of feasible low frequency energy harvesting sources and applications.

KEYWORDS: series and parallel SSHI

Introduction:

The most common method of harvesting vibration energy from piezoelectric elements is shown in fig.1. A piezoelectric generator has a blocking output capacitance which is connected to a diode full bridge rectifier. This is throughout the project known as the standard full bridge, and abbreviated STD. When the piezoelectric output voltage is greater than the output capacitor voltage + diode bridge forward voltage, energy is harvested.

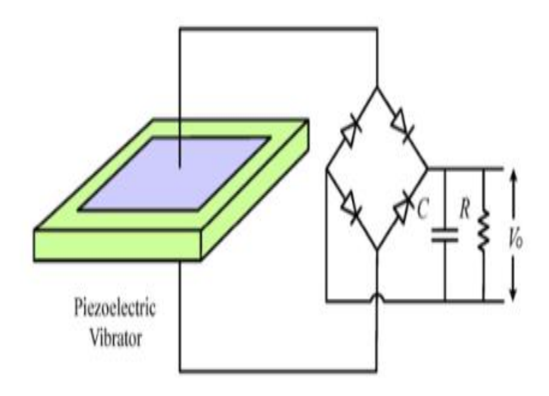


Figure.1: PVH with commonly used rectifying circuit.

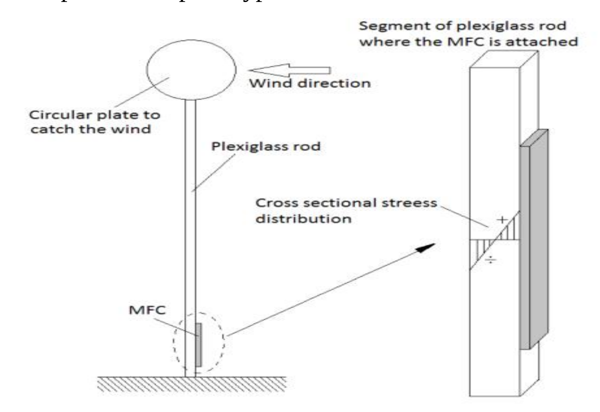
1.2 Energy Harvesting Application:

The vibrational energy harvested in this project is supplying a sensor node, but can in general be used wherever there is low frequency vibrations and low power electronics.

The sensor node being developed at the Danish company DELTA is a small computing device capable of collecting data, joining a mesh network and through this transmitting its data to a base station. A mesh of such nodes is known as a sensor network. Such sensor nodes are usually supplied with power from batteries, but these require maintenance. To avoid this, the nodes can be made energy self-sufficient by means of energy harvesting. The sensor node needs an energy amount of 680 µJ to perform a cycle of start up, sensor measurement and data transmit.

2. Wind-Spear Structure design used in simulation:

One application is the Wind-Spear developed at DELTA. This consists of a plexiglass rod stuck into the ground with a circular plate on the top which increases the air resistance and makes the rod bend in the wind as illustrated in fig.2. A MFC piezoelectric material is mounted on the sides of the spear. When the wind blows, just a gentle breeze around 1 m/s, the spear bends and vibrates around its resonance frequency of 1 Hz and energy is generated in the piezoelectric material. The top end of the Wind- Spear is in this case vibrating with displacement amplitude ~ 1 cm and this corresponds to a displacement of the piezoelectric element ~ 1 mm. This generates an open circuit voltage of 8 V, which is used as example throughout the project. The generated energy is harvested to supply the sensor node. The sensor node will in this application monitor climate and environmental data. The power level at this vibration amplitude and frequency is however very low, e.g. in the microwatt range. Thus there is a need for optimizing the output power. The MFC piezoelectric material mounted on the Wind-Spear has a capacitance measured to be C_p= 42 nF. This capacitance is an important parameter which will be used throughout the whole project. The WindSpear will in the end of this project serve as test application for evaluating the implemented prototype.



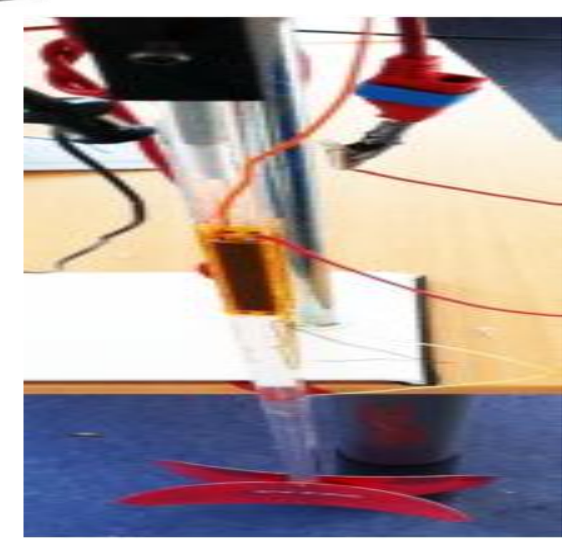


Figure. 2(a): Wind-Spear mounted in hanging configuration for the prototype test.



Figure. 2(b): DC motor is in connection with the end of the Wind-Spear via the green stick and makes it vibrate at frequency of 1.2Hz.

3. Synchronized Switch Harvesting on Inductor (SSHI):

In fig.3 (a) the P-SSHI circuit schematic is seen and in fig.3 (b) the S-SSHI circuit schematic is seen. The only difference between them is the placement of the rectifying bridge with the output. A photo of the P-SSHI prototype is seen in fig.3(c).

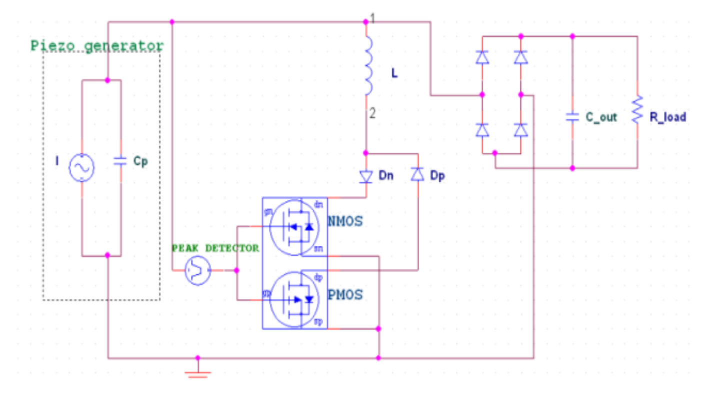


Figure.3(a): Simplified PSpice simulation circuit for analyzing the P-SSHI topology.

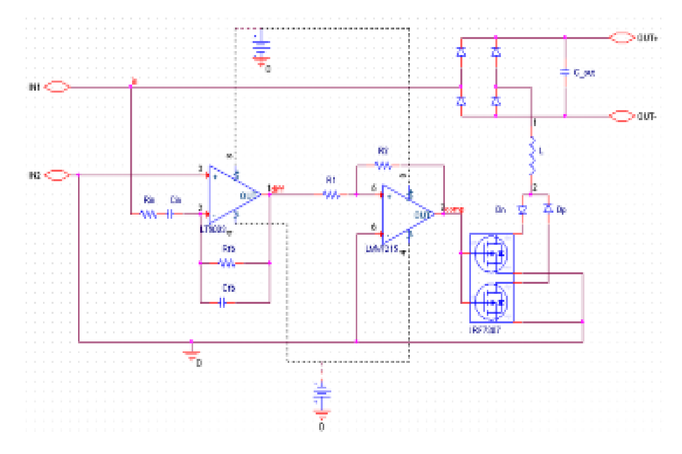


Figure.3 (b): Simplified PSpice simulation circuit for analyzing the S-SSHI topology.

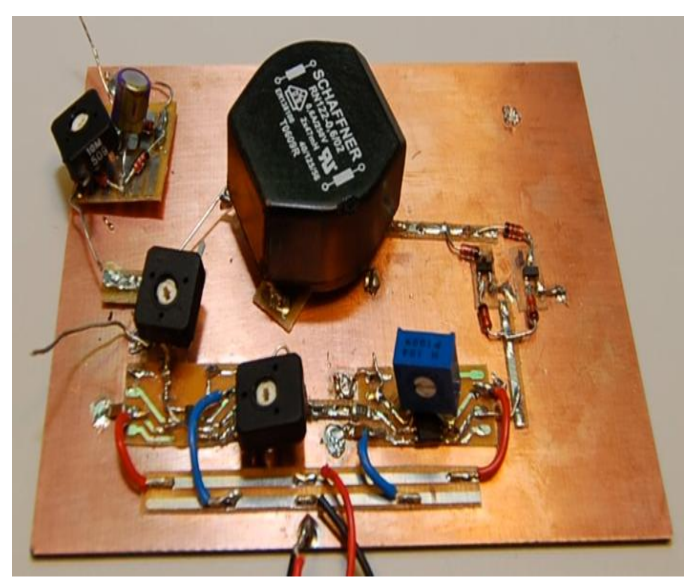


Figure. 3(C): Implemented P-SSHI prototype.

4. RESULTS:

This topic will describe the measurements of the implemented circuit tested with the Wind-Spear. The circuit can be configured both as Series-SSHI and Parallel-SSHI just by placing the inductor in series or parallel with the piezoelectric element. The prototype performance is illustrated and compared with the expectations. The power consumption of the control circuit is estimated and the output power increase results are evaluated, stating which parts of the circuit could be optimized.

4.1 Wind-Spear Test:

The spear is mounted upside down, hanging from a fixture and vibrated by a 1.2 Hz motion created by a DC engine, simulating a light wind breeze (photos of the hanging Wind-Spear can be seen in figure 3a&3b).

Fig. 4.1 shows a measurement of the open circuit piezo voltage. This is estimated to V_p = 7.6 V. The waveform is uneven due to the mechanical setup non-idealities.

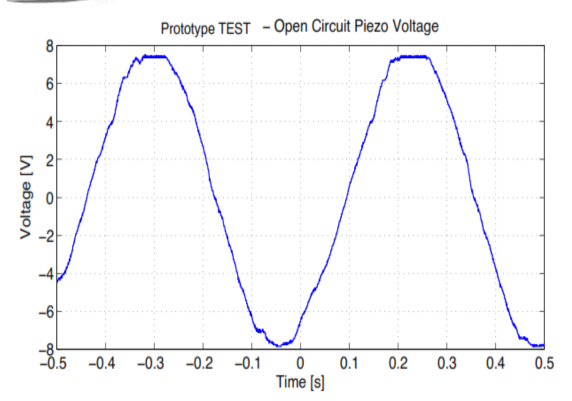


Figure. 4.1: WindSpear open circuit piezo voltage.

4.1.1 Parallel-SSHI:

The piezo voltage of the P-SSHI circuit in operation is seen in fig. 4.2. If it is assumed that the voltage peak (optimum switch time) is just before the voltage starts to decrease, it is seen that the voltage inversion happens a short while after. It is estimated that the vibration period is T = 0.54 s ~ f = 1.2 Hz and the inversion happens $t_2 \sim t_1$ = 0.07s after the peak. This time delay is above the limit of 0.05s, and might cause less power output. The inversion factor is from fig.4.2 estimated to be $\gamma = -\frac{V_{g+}}{V_{g-}} = -\frac{1.2V}{-3.4V} = 0.35$. This could be higher and this is just at the boundary of when the circuit increases the total output power.

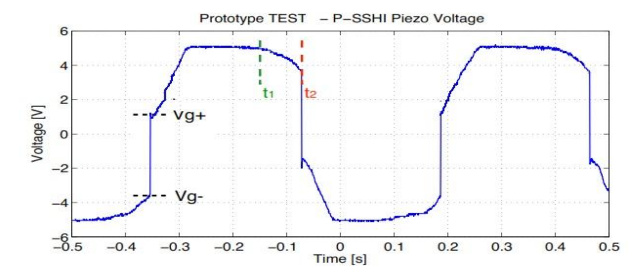


Figure. 4.2: P-SSHI piezo voltage with an output load of R = 2.7 MΩ. The voltage peak is a t1 and the actual inversion happens a t2 .The inversion factor is estimated to be $\gamma = -\frac{V_{g+}}{V_{g-}} = 0.35$.

Table.1 shows the main parameters of the P-SSHI circuit test.

MOSFETs Inductor Load	IRF7307 (C_{oss}=300pF) L = 180 mH R = 2.97 MΩ
Inversion factor Time delay	$\gamma = 0.35$ $t_d = 5mS$

Inversion: In fig.4.3 the inductor inversion voltage is seen, where the PMOS turns ON and initiates the inversion.

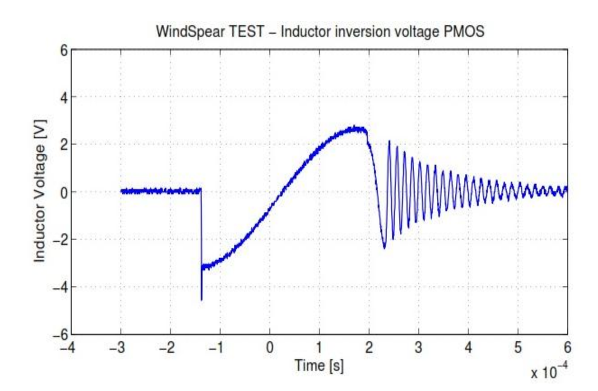


Figure. 4.3: P-SSHI inductor inversion voltage when PMOS turns ON. The load connected is R=2.7 MΩ.

4.1.2 Series-SSHI:

The piezo voltage for the S-SSHI circuit test is seen in fig. 4.4. The test parameters are seen in table.2. The inversion factor is estimated to be $\gamma = -\frac{-1.5V}{7V} = 0.21$. this is significantly lower than the P-SSHI inversion factor. The main reason is found to be the inductor series resistance. When the S-SSHI circuit is switching the inductor in series with the piezo capacitor, power is delivered to the load. The rest of the time, the piezoelectric element is in open circuit. This means that every time the power flows to the load, it has to go through the inductor, and thus through the inductor series resistance, where power is lost.

Table.2 S-SSHI Test Parameters

MOSFETs Inductor Load	IRF7307 (C_{oss}=310pF) L = 180 mH R = 1.6 MΩ
Inversion factor Time delay	$\gamma = 0.21$ $t_d = 5mS$

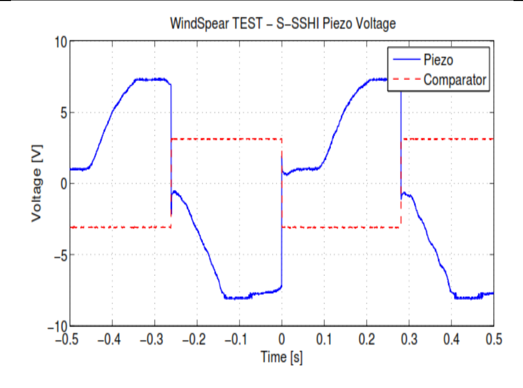


Figure. 4.4: S-SSHI piezo voltage and comparator output with load R = 1.6 MΩ

Inversion: in fig.4.5 the inductor inversion voltage when NMOS turns ON is seen. To show the resonance dependency on the MOSFET output capacitance.

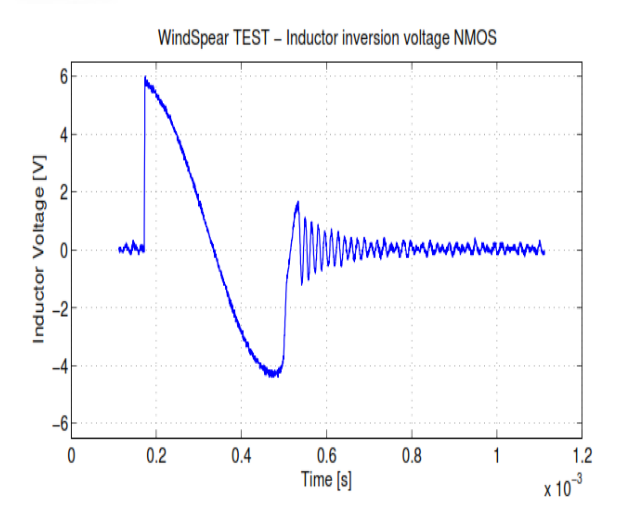


Figure. 4.5 S-SSHI inductor inversion voltage when PMOS turns ON.

4.2 Peak Detection Method:

To show the effect of switching the SSHI inductor ON before and after the optimal in- stance, a test was made where the piezoelectric element was vibrated at 1 Hz and an external square wave control signal controlled the MOSFETs slightly off-set at 1Hz. The P-SSHI circuit used was loaded with a resistive load. this test shows in fig.4.6. the inversion dependence of when the MOSFETs are switched ON. The inversion factor in the test is low, but the purpose is to show its dependence on the peak detection. It shows the effect of switching ON the inductor before the capacitor current has reached zero, i.e. there is still current flowing in to the piezo capacitor charging the voltage again. This creates the small voltage bumps seen after the switching. When the switching occurs at the moment where the current into the capacitor is zero, i.e. the optimal time, the voltage bump is not seen. There are no bumps as well, when the piezo is switched after the optimal time late but the inversion is reduced.

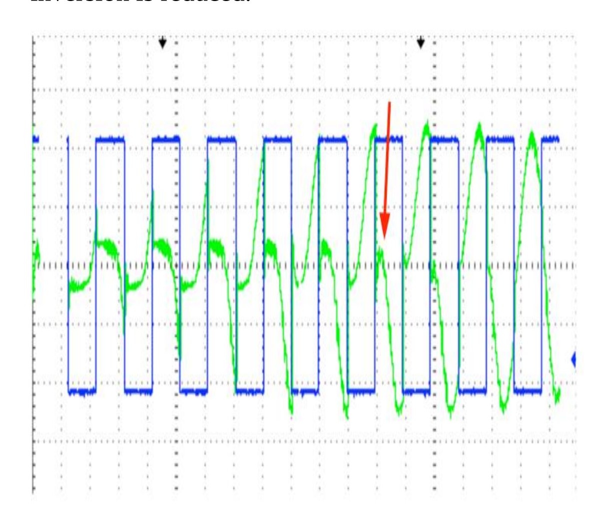


Figure. 4.6: Piezo generator vibrating at 2 Hz and SSHI circuit with 1 Hz external control signal slightly off sync. Shows dependence on when the switching is done and that it needs to be a bit after the voltage peak due to reduced phase shift when resistive loading of the piezo. Red arrow indicates voltage bump after switching directly on the voltage peak. The missing time/voltage scale is 250 ms/div and 2 V/div and the figure is two merged oscilloscope screenshots.

Voltage bumps seen on the graph corresponds to the piezo capacitance getting charged again by the current left in the source but only up until a diode forward voltage drop due to the blocking diode, D_n or D_p. The explanation for why the optimum switching instance in this test is after the voltage peak can be explained by the resistive load. When the piezoelectric element is in open circuit it can be seen as only having a capacitive load consisting of its output capacitance. Here the phase shift between the current and the voltage is -90^0. When applying a resistive load, this phase shift is decreased. That results in shifting the optimum switching instance after the voltage peak, as shown in fig.6. The main challenge with the peak detection circuit used in the prototype is the balance between the phase shift and the gain. The gain is -20 dB at 1 Hz. adjusting the feedback component values can increase the gain but will decrease the phase shift. The optimal point for switching the inductor ON, is when the current in the piezo capacitor is zero. This happens when the piezoelectric element reaches its maximum displacement. When it is loaded with a resistive load, the phase shift between the current and the voltage will not be exactly 90^0, but less. The piezoelectric generator does not only see its internal capacitance as it does in open circuit, but the external resistive load makes the phase shift decrease. This will only be an issue with the parallel SSHI circuit as the load is connected to the piezoelectric element all the time. In the series-SSHI, the load is only intermediately connected, when switching, and the rest of the time the piezoelectric element is left in open circuit and the phase shift will thus not be affected by the resistive load.

For optimal control one would need a zero current detector. This is although not feasible. The optimum switching instance shift in P-SSHI can instead be solved by using a small secondary piezoelectric element only for the control. This will not be loaded and the thus the voltage peak will precisely correspond to the extremum displacement, which correspond to the instance with zero piezo capacitor current.

4.3 Power Results:

The measurement results of the prototype output power are seen in fig. 4.7. Here the P-SSHI and the S-SSHI prototype results are shown together with measurements of a standard full bridge with 4 diodes (1N4148) and $C_{OUT} = 10\mu F$. It is seen that the P-SSHI circuit does increase the power output of the piezoelectric element in comparison to STD by up to a factor of 2. S-SSHI however does not and the reason for this is mainly the low inversion factor.

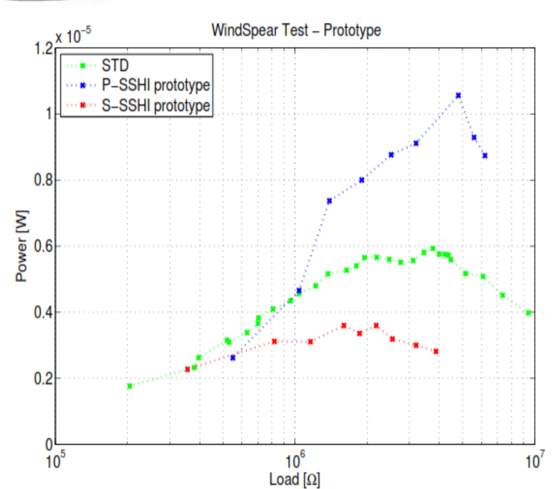


Figure. 4.7: Measurement results of the Parallel-SSHI and Series-SSHI prototype along with the standard full bridge, STD.

4.4. Prototype Evaluation:

To evaluate the measurement results, the expected theoretical power output of the SSHI circuits with the realized inversion factors from the test, are shown in fig.4.8.

One has to keep in mind that the power levels are very low at 1 Hz. e.g. force applied, is dependent on the frequency squared. The Wind-Spear is operating around 1 Hz due to its structure. To give an impression of when the prototype in theory would produce more power than the standard bridge.

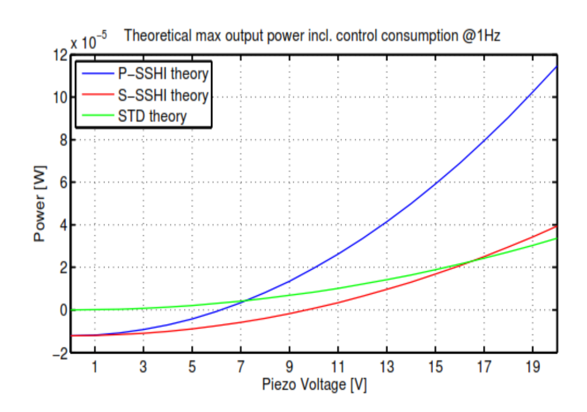


Figure. 4.7: Theoretical maximum output power of P-SSHI (γ =0.35) and S-SSHI (γ =0.21) with the estimated control power consumption subtracted. Compared with the maximum output power of the standard full bridge for vibrations at 1 Hz as a function of the piezo open circuit voltage, V_p.

It is seen that the P-SSHI gives a net power output increase when operating with piezo voltages $V_p > 7V$, in comparison to STD, corresponding to an output power of 5µW. The S-SSHI inversion factor is very low and is thus not expected to deliver a power increase, before a piezo open circuit voltage $V_p > 17V$, corresponding to an output power level of 25 µW. At this level the P-SSHI circuit is expected to output 80µW. This shows the importance of the inversion factor. The losses in the inductor and the diode were found to be the in order of the output power, and it is concluded that further optimization should focus on these parts. Especially the inductor loss should be simple to reduce by a lower series resistance inductor.

5. CONCLUSION:

A prototype was implemented both as a series and a parallel version of the SSHI topology. The prototype was tested with Macro Fiber Composite piezoelectric(MFCP) material mounted on a vibration harvesting device called the Wind-Spear, and the results showed that the prototype Parallel-SSHI circuit increased the power output of the piezoelectric material to 11 µW compared with the standard full bridge rectifier of 5.9µW. Though, since the power consumption of the control circuit was higher than the prototype output power, the total net output power of the SSHI prototype was lower than the standard full bridge. T he power output from the prototype was lower than expected due to a low inversion factor. The limiting components were evaluated and along with the losses in the oscillation path, primarily the loss in the diode and the series resistance of the inductor, the peak detection control circuit was found to be the main reason for the low inversion factor. The control circuit was expected to make the circuit switch at every voltage peak with a time delay of 12 ms, but was found being incapable of this due to a low gain in the differentiator. The control circuit feedback was thus modified which caused an increased time delay to 70mS. The time delay made the circuit perform the switch after the optimal point, which is assumed to be the main factor decreasing the power output of the prototype circuit. And also this work has investigated the SSHI topology potential at low frequencies, and it was seen that low frequency vibration harvesting is challenging at power levels of microwatts, mainly since the power consumption of the control circuit also is in the microwatt area. When considering a full energy harvesting system another DC/DC converter is needed for matching the load and this will introduce additional power consumption. At higher vibration levels the prototype is expected to increase the power output significantly.

6. References:

i. *A. Badel, M. Lagache, D. Guyomar, E. Lefeuvre, and C. Richard. Finite element and simple lumped modeling for flexural nonlinear semi-passive damping .Journal of intelligent Material Systems and Structures ,18:727{742 ,2007.*

ii. *A. Badel, G. Sebald D. Guyomar, M. Lallart, E. Lefeuvre, C. Richard, and J. Qiu. Piezoelectric vibration control by synchronized switching on adaptive voltage sources: Towards wideband semi-active damping. Acoustical Society of America, 2006.*

iii. *Edited by Mickal Lallart. Ferroelectrics - Applications. InTech, 2011.*

iv. *Anantha Chandrakasan, Rajeevan Amirtharajah, James Goodman, and Wendi Rabiner. Trends in low power digital signal processing. Department of EECS, Massachusetts Institute of Technology, Cambridge, 1998.*

v. *Thomas P. Daue, Jan Kunzmann, and Andreas Schoenecker. Energy harvesting systems using piezo-electric macro fiber composites. Smart Material Corp., 2008.*

vi. *Shashank Priya and Daniel J. Inman (editors). Energy Harvesting Technologies. Springer, 2009. ISBN: 978-0-387-76463-4.*

vii. *Yogesh K. Ramadass and Anantha P. Chandrakasan. An efficient piezoelectric energy harvesting interface circuit using a bias-flip rectifier and shared inductor .IEEE Journal of solid-state Circuits ,45(1) ,2010*

viii. *Bjorn Baruel Petersen. Apparatdesign til vibrations- og chokkrav. enkle overslagsberegninger, formler, eksempler og regler. DELTA, 1987.*